

Rapid Convergence to Feature Layer Correspondences

Jörg Lücke¹, Christian Keck², and Christoph von der Malsburg³

¹ Gatsby Computational Neuroscience Unit, UCL
London WC1N 3AR, UK

² Institut für Neuroinformatik, Ruhr-Universität Bochum
44780 Bochum, Germany

³ Frankfurt Institute for Advanced Studies, Goethe-Universität Frankfurt
60438 Frankfurt am Main, Germany

Abstract

We describe a neural network able to rapidly establish correspondence between neural feature layers. Each of the network's two layers consists of interconnected cortical columns and each column consists of inhibitorily coupled subpopulations of excitatory neurons. The dynamics of the system builds upon a dynamic model of a single column, which is consistent with recent experimental findings. The network realizes dynamic links between its layers with the help of specialized columns that evaluate similarities between the activity distributions of local feature cell populations, are subject to a topology constraint, and can gate the transfer of feature information between the neural layers. The system can robustly be applied to natural images and correspondences are found in time intervals estimated to be smaller than 100 ms in physiological terms.

Keywords: Cortical Columns, Homomorphy, Non-linear Dynamics, Correspondence Problem, Visual Cortex, Dynamic Links

1 Introduction

Aristotle described two kinds of mental association: by time and by pattern (*The Complete Works of Aristotle*, Barnes (ed.), 1984). It is interesting to note that standard neural network theory, which sees association by time implemented as Hebbian plasticity, has no sophisticated and direct concept of association by pattern. In standard approaches, a common way to link two patterns is to compactly represent them by cardinal cells, which can then be associated by time, but only if external events activate the patterns simultaneously. Thus, structural relations between patterns as such cannot lead to association directly.

A mechanism that enables association by pattern requires a concept of pattern similarity and, for complex patterns, similarity is best formulated as homomorphy: A pattern is composed of elements that carry feature labels and that have neighborhood relationships. Two patterns are homomorphic if there is a mapping between them that relates elements with similar labels such that neighbors are mapped onto neighbors. The process of establishing such a mapping is often referred to as *matching*.

In the context of vision, homomorphic pattern matching is important to find stereo correspondences (i.e. finding point-to-point relationships between the two retinal images), for motion extraction (finding correspondences between consecutive images), and for pattern recognition (finding correspondences between retinal images and patterns in memory). Systems that apply explicit pattern matching mechanisms are state-of-the-art in object and face recognition technology (Phillips et al., 2000; Messer et al., 2004). More generally, pattern associations are probably fundamental for subsystem integration in the brain and for intelligence in general, where new problems are solved by homomorphy to known problems or to abstract schemas.

It has repeatedly been proposed to expand standard neural networks by the introduction of a class of neural units that stand not for pattern elements but that stand for relationships between pattern elements. The general idea is formulated in (Kree and Zippelius, 1988), application to stereo matching in (Dev, 1975; Marr and Poggio, 1976), and application to correspondence-based object recognition, e.g., in (Hinton, 1981; Olshausen et al., 1993; Wiskott and von der Malsburg, 1995; Arathorn, 2002; Zhu and von der Malsburg, 2004). These systems are non-standard in requiring unusual interaction patterns to implement estimation of label similarity, topographic relations and for controlling the flow of signals between the matched patterns.

The model we present here builds on previous neural network approaches such as (Hinton, 1981; Olshausen et al., 1993; Wiskott and von der Malsburg, 1995). The model described in (Hinton, 1981) represents an early conceptual study. The model in (Olshausen et al., 1993) represents an analytically and numerically well-investigated correspondence-based approach that is, however, limited to scalar features types and artificial input. The model in (Wiskott and von der Malsburg, 1995) uses more advanced features and realistic input but has problems to neurally explain feature similarity evaluation and it cannot account for the speed of human object recognition as measured by Thorpe et al. (1996).

The neural network model studied in this work addresses these deficits of previous models. We use a neuro-dynamic approach that reflects recent results on cortical connectivity (e.g. Douglas and Martin, 2004; Yoshimura et al., 2005) and implements pattern matching using neural populations as elementary computational units. We find that the network model can (1) establish pattern correspondences in physiologically plausible times (< 100 ms) and can (2) be applied robustly to natural images. Using a specific neural circuitry to organize the interplay between feature similarities and feature arrangements, the model overcomes the time-limitations in earlier neural models (e.g. Wiskott and von der Malsburg, 1995) and limitations to scalar features and artificial inputs as used in (Olshausen et al., 1993).

The paper is structured as follows: In Sec. 2 we introduce and discuss a dynamic

model of a single cortical column as formulated in (Lücke, 2005), and subsequently introduce the architecture of our network model which consists of two layers of such columns. The dynamics of the layers and their principle interaction is defined and discussed in Sec. 3. Sec. 4 describes how feature arrangements are neurally evaluated and Sec. 5 gives details of the Gabor-features used. In Sec. 6, numerical simulations show the system's dynamic behavior and its convergence to pattern correspondences if natural images are used as input. Sec. 7 discusses the system's properties and its relation to the literature.

2 Columnar Network Model

The central element of our model is the *cortical column*. Depending on the perspective or the cortical area a column is also often referred to as macrocolumn (Mountcastle, 1997), segregate (Favorov and Diamond, 1990), or hypercolumn (Hubel and Wiesel, 1977) and in primary visual cortex comprises roughly all neurons that can be activated from one point in visual space. In recent neurophysiological experiments it was shown that columns possess a fine-structure of relatively disjunct sub-populations of excitatory neurons (Yoshimura et al., 2005). A model of a column with this structure was studied in (Lücke and von der Malsburg, 2004; Lücke, 2004) and we will base our system on an abstract dynamical formulation as suggested in (Lücke, 2005). This abstract formulation models the mean activity in populations of

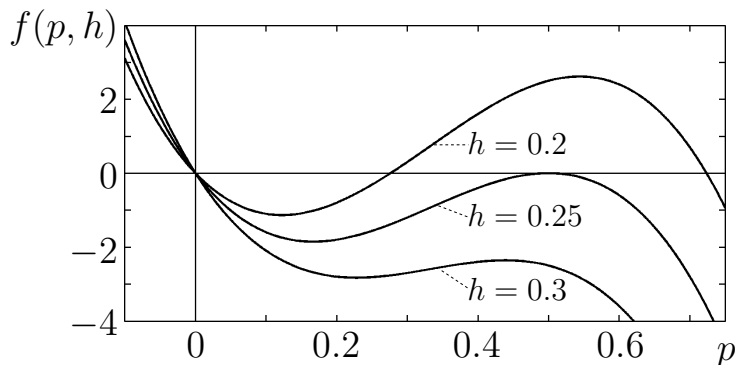


Figure 1: Plot of the function $f(p, h)$ in (1) for three different values of h and $\sigma_n = 0$. The function models the behavior that is expected from a population of interconnected excitatory neurons with inhibitory input h . If $\frac{d}{dt}p = f(p, h)$ describes the change of activity p in such a population than f results in two stable stationary points if h is small: one at zero and one with high activity. The activity is increased if $f(p, h) > 0$ and decreased if $f(p, h) < 0$. Values are plotted for $a = 100$ (unit omitted) but note that just the scale of the y -axis changes for other values of a .

excitatory neurons. To recapitulate the approach in (Lücke, 2005), consider a single population of excitatorily interconnected neurons. Through its connections, such a

population can be expected to increase its activity level. From a critical level of activity on, active neurons in one time interval can excite an increasingly large number of neurons in the next time interval. This positive feed-back loop continues until the self-excitation is counterbalanced by self-inhibition, e.g., through neural refraction times. If activity in the population is very low, excitatory neurons are not able to excite a larger number of other neurons. In this case we expect the activity to decay to zero. If the change in activity is described by a differential equation $\frac{d}{dt} p = f(p, h)$ with p denoting the population's mean activity, we can model this expected dynamic behavior using a polynomial of order three for f :

$$f(p, h) = a(p^2 - hp - p^3) + \sigma_n \eta_t. \quad (1)$$

In (1), $\sigma_n \eta_t$ is additive Gaussian noise of variance σ_n^2 , which models noisy activities that are to be expected. The linear term $-hp$ models the influence of external inhibition h : the effect of inhibition increases the more neurons are active, for no activity inhibition is without effect. Fig. 1 depicts the function f for three different values of h and no noise. As can be observed, a population can only stabilize high levels of activity if the level of inhibition is small. For high levels, the population activity converges to zero.

The column model used in this paper consists of k populations of excitatory neurons that are coupled inhibitorily. Measurements reported in (Yoshimura et al., 2005) suggest that such a model reflects the fine-scale structure within a cortical column. Pyramidal cells in layer 2/3 of the visual cortex were found to form functionally disjunct populations that receive a common inhibition from within their layer. Here, we will model this lateral inhibition to be proportional to the maximally active population in the column: $h = h(p_1, \dots, p_k) = \nu \max_{\alpha} \{p_{\alpha}\}$, where p_{α} denotes the activity in population or *unit* α of the column. Different types of inhibitory coupling were studied (see, e.g., Lücke et al., 2002; Lücke and von der Malsburg, 2004) but inhibition proportional to the maximal activity has been found to have a number of functional advantages (Lücke, 2005). Taken together, the dynamics of a column is described by the equation system:

$$\frac{d}{dt} p_{\alpha} = f(p_{\alpha}, \nu \max_{\beta=1, \dots, k} \{p_{\beta}\}) + \kappa \tilde{\mathcal{J}}_{\alpha}, \quad (2)$$

where the $\tilde{\mathcal{J}}_{\alpha}$'s are external inputs to the $\alpha = 1, \dots, k$ different units. κ parameterizes the coupling strength of the column dynamics to the input. As a neuron within a population is found to receive most of its input from within its own population (Yoshimura et al., 2005), κ will later (Sec. 6) be set to a value which is small compared to a in (1).

In this paper a multitude of columns of the type above constitute neural layers for the representation of input and model images. A simple model setting for the process of correspondence finding (see Fig. 2A) consists of an *input layer* \mathcal{I} , left array of large shaded ellipses, and a *model layer* \mathcal{M} , right array. Both layers represent images by activity distributions in local feature-sensitive populations and will therefore be referred to as *feature layers*. The model domain should contain many such feature

layers to represent objects in memory, but in this work we focus on just one. Note that for visualization purposes the layers in Fig. 2A are displayed one-dimensionally. In each point of the two layers there are two columns, one to represent local features (horizontal ellipses within the shaded regions of Fig. 2A) and one (vertical ellipse) to control the connections or *links* between the two layers. This double column (a shaded ellipse in Fig. 2A) is called a *node*. *Feature columns* represent, with their activity, the local textures of the input or model images. Different activity levels in their units encode for different local spatial frequencies and orientations of an image’s gray-level distribution, details of which will be given later in Sec. 5.

As will be discussed at the end of the paper, the feature layers can be thought of as different areas in the visual cortex. They communicate through links, which connect feature columns by as many fibers as there are feature types. In a *link control column* each unit stands for one link entering the node and does three things. One, it compares the activity distributions of the feature columns at the two ends of the link, two, it tries to be consistent with activities of units controlling parallel links (“topology constraint”), and three, by its activity it keeps open its link. The situation is shown in more detail in Fig. 3A. As we will see later, the dynamics of the system results, per column, in the deactivation of all but one control unit, i.e., all but one of the links into a node are switched off. The link that remains active is selected by a combination of two criteria. One is feature similarity, the other is the topology constraint. The latter is to favor those link arrangements that connect neighbors in one layer with neighbors in the other layer, and is implemented by connections between control units in neighboring nodes (see Fig. 2B). The topology constraint is important when feature similarities are ambiguous and would, on their own, lead to many wrong correspondences. For a systematic study of the influence of the topological constraint see (Wiskott, 1999).

3 System Dynamics

The dynamics of the system builds upon the column model given by (2). The dynamic properties of single columns and the specific connectivity outlined in the previous section define the dynamic properties of the whole network. We first introduce some notation. Let $\mathcal{L} \in \{\mathcal{I}, \mathcal{M}\}$ and $\mathcal{L}' \in \{\mathcal{I}, \mathcal{M}\} \setminus \{\mathcal{L}\}$ be indices for the two layers, i.e., $(\mathcal{L}, \mathcal{L}') = (\mathcal{I}, \mathcal{M})$ or $(\mathcal{M}, \mathcal{I})$. Further, let $p_\alpha^{\mathcal{L}i}$ stand for the activity of the feature unit α in node i of layer \mathcal{L} (Fig. 3B). We assume α to run from 1 to k and i from 1 to N , where N is the number of nodes per layer. Using the column model (2), the dynamics of the feature columns is described by

$$\frac{d}{dt}p_\alpha^{\mathcal{L}i} = f(p_\alpha^{\mathcal{L}i}, \nu \max_{\beta=1, \dots, k} \{p_\beta^{\mathcal{L}i}\}) + \kappa \tilde{\mathcal{J}}_\alpha^{\mathcal{L}i}, \quad (3)$$

where $\tilde{\mathcal{J}}_\alpha^{\mathcal{L}i}$ is feature input to the unit α of node $\mathcal{L}i$. A feature column represents a given feature vector $(\tilde{\mathcal{J}}_1^{\mathcal{L}i}, \dots, \tilde{\mathcal{J}}_k^{\mathcal{L}i})$ by activities of its k sub-populations. The feature vectors can convey information from the other layer and from an (input or model) image. The importance of input from the other layer lies in the transmission

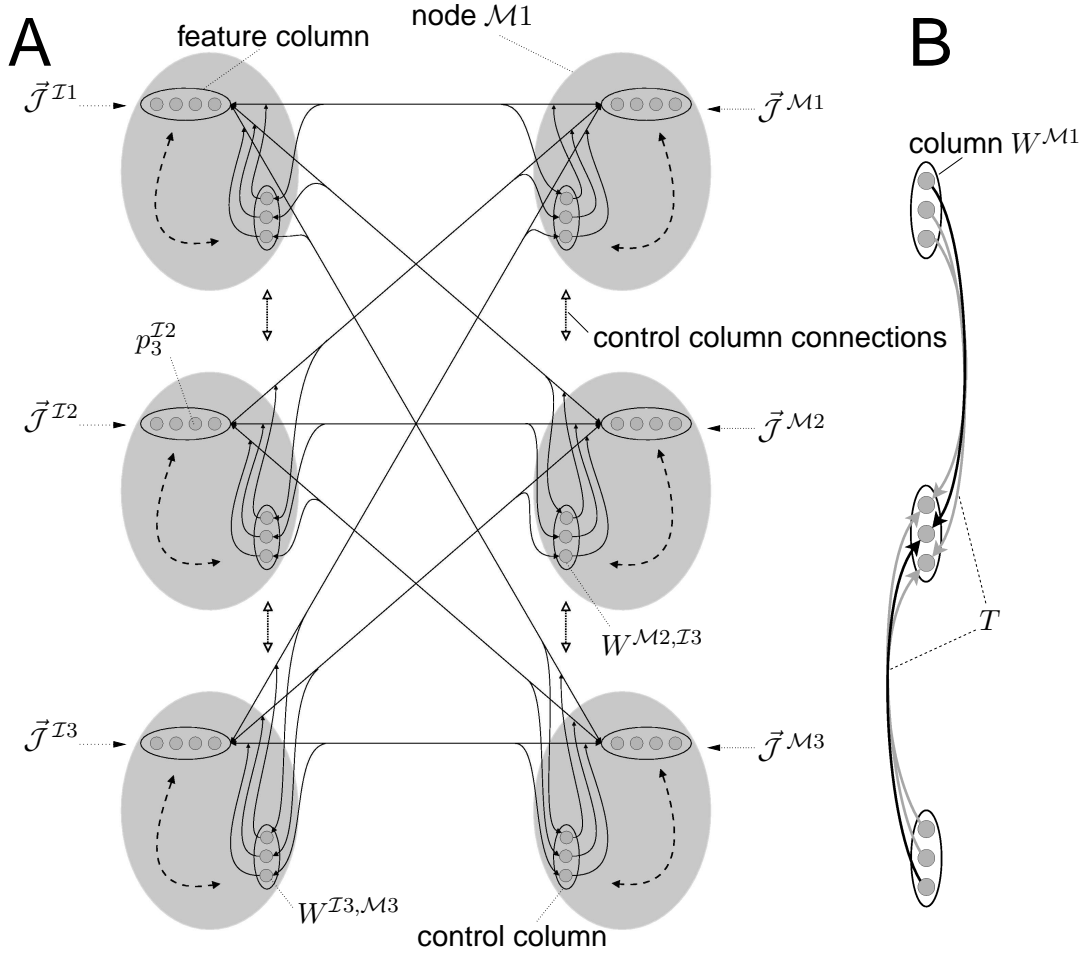


Figure 2: **A** Network of columns for correspondence finding. The network consists of an input layer and a model layer with nodes $\mathcal{I}1$ to $\mathcal{I}3$ and $\mathcal{M}1$ to $\mathcal{M}3$, respectively. Each node consists of a feature column (horizontal ellipse) with $k = 4$ units and of a control column (vertical ellipse) with $N = 3$ units. Each node in the input layer receives input from each node in the model layer, and *vice versa*. The inputs to a node are modulated by its control column according to the interconnectivity as displayed in Fig. 3. The control columns receive input from the units of feature columns of both layers and from neighboring control columns. **B** Input received by control column $W^{\mathcal{M}2}$. Units that control parallel links excite each other. The interconnectivity implements cyclic boundary conditions.

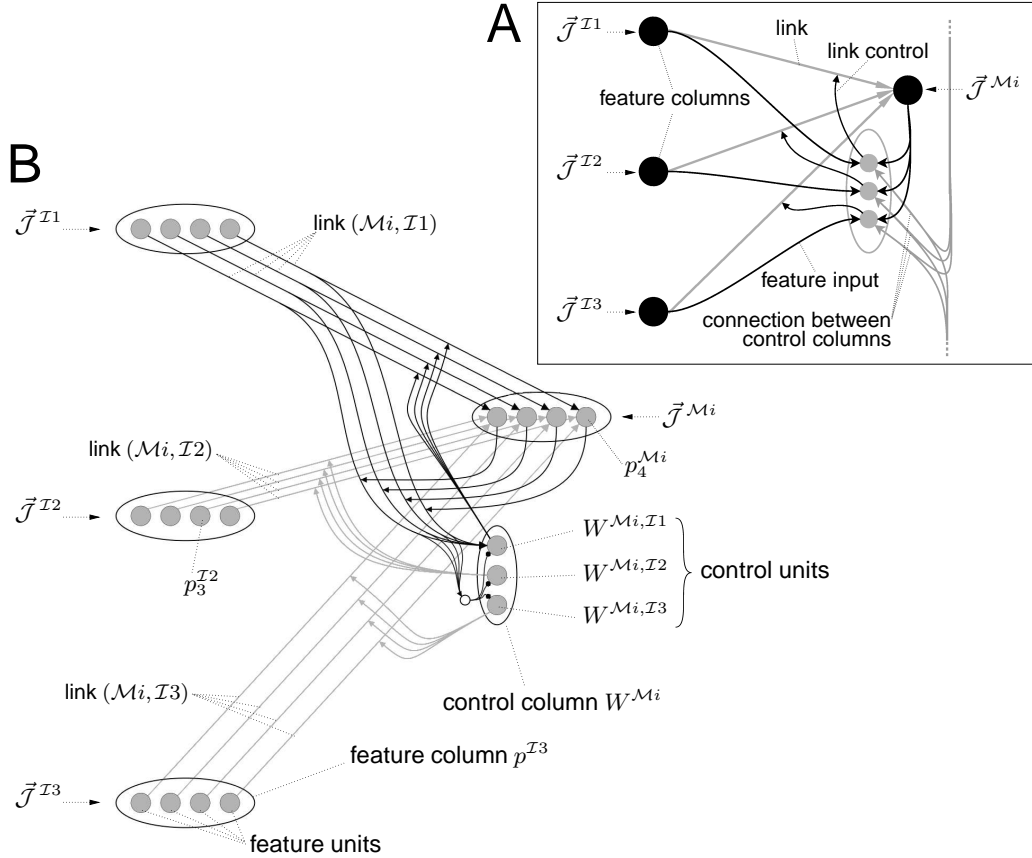


Figure 3: Detailed connectivity of one model node. The node \mathcal{M}_i consists of a feature column and a control column. On the input side, only the feature columns of the input nodes are shown. The feature vectors $\vec{\mathcal{J}}^{\mathcal{I}j}$ (on the input side) and $\vec{\mathcal{J}}^{\mathcal{M}_i}$ (on the model side) are represented by the activity distributions in their feature columns. Images **A** and **B** illustrate the connectivity of the model node at different resolutions. In **A** the information that converges onto the node's control column is shown together with the controlled links. Input to each control unit is a mixture of, one, feature inputs from different layers and, two, inputs from neighboring control columns of the same layer. For details about the connections that convey the latter type of input see Fig. 4. The control column has as many units as there are nodes in the input layer, in order to control as many links. A given control unit integrates feature information from the pair of feature columns that is associated with its link and from neighboring control columns. In **B** the connectivity of the model node is shown in more detail and together with labels for the system's dynamic variables as they appear in (3) to (5). Connections from other control columns are not shown. The control units evaluate the similarity between feature column activities in terms of the scalar product of their activity vectors (multiplicative interactions indicated by arrowheads touching connecting fibers). With its output a control unit gates the incoming link it stands for. Linking fibers are depicted as feature preserving. The small circle represents neurons that, by inhibition, subtract the mean from incoming feature inputs.

of information after correspondences have been established. In that situation the information is channeled through the links between the layers that connect corresponding points, and it is the task of the control columns to select these links. In this paper we study the neural dynamics of link selection, for which the direct connections between feature columns are not required. For simplicity, the inputs in (3) will therefore convey information from the (input or model) image alone (see Lücke and von der Malsburg, 2006, for a system with about an equal mixture of image input and input from the other layer). Details of the image features will be given in Sec. 5.

For the control columns we use the same dynamic model as for the feature columns. To allow for potentially all possible connection patterns between the layers, each control column must contain as many control units as there are nodes in the other layer, in order to control as many links (see Fig. 2A and Fig. 3A). The control column of node $\mathcal{L}i$ will be referred to as $W^{\mathcal{L}i}$ and the activity in its units will be denoted by $W^{\mathcal{L}i,\mathcal{L}'j}$ with $j = 1, \dots, N$ (see Fig. 3B). A unit $W^{\mathcal{L}i,\mathcal{L}'j}$ controls the link from node $\mathcal{L}'j$ in layer \mathcal{L}' to node $\mathcal{L}i$ in layer \mathcal{L} . The link is open or active if and only if its unit is active. The activity distribution within a control column, $W^{\mathcal{L}i}$, represents the current connectivity of node $\mathcal{L}i$ to nodes of the other layer. The distribution is determined by the dynamics within the control column and by its inputs $I^{\mathcal{L}i,\mathcal{L}'j}$:

$$\frac{d}{dt}W^{\mathcal{L}i,\mathcal{L}'j} = f(W^{\mathcal{L}i,\mathcal{L}'j}, \nu \max_{l=1,\dots,N} \{W^{\mathcal{L}i,\mathcal{L}'l}\}) + \kappa I^{\mathcal{L}i,\mathcal{L}'j}, \quad (4)$$

$$I^{\mathcal{L}i,\mathcal{L}'j} = C_I \underbrace{\sum_{\alpha,\beta=1}^k p_{\alpha}^{\mathcal{L}i} R_{\alpha\beta}^{\mathcal{L}i,\mathcal{L}'j} p_{\beta}^{\mathcal{L}'j}}_{\text{similarity term}} + (1 - C_I) \underbrace{\mathcal{T}^{\mathcal{L}i,\mathcal{L}'j}}_{\text{topology term}}, \quad (5)$$

where $C_I \in [0, 1]$ controls the relative influence of the two terms in (5). The first term evaluates feature information represented by feature columns $p^{\mathcal{L}i}$ and $p^{\mathcal{L}'j}$, which is conveyed by the afferents ($R_{\alpha\beta}^{\mathcal{L}i,\mathcal{L}'j}$) to control unit $W^{\mathcal{L}i,\mathcal{L}'j}$. We use for all control units the same connectivity structure and choose $R_{\alpha\beta}^{\mathcal{L}i,\mathcal{L}'j} = \delta_{\alpha\beta} - \frac{1}{k}$. In this case the similarity term resembles a scalar product with Euclidean metric between the activity vectors of the two associated feature columns $p^{\mathcal{L}i}$ and $p^{\mathcal{L}'j}$ (other choices of $R_{\alpha\beta}^{\mathcal{L}i,\mathcal{L}'j}$ would correspond to other metrics). The second term in (5) implements the interaction between control columns within a layer, which will be used to enforce the topological constraint (Sec. 4). The connectivity of a single control column is illustrated in Fig. 3.

If equations (3) and (4) are numerically simulated, we find that the dynamics possesses, for a wide range of parameters, a number of point attractors that grows exponentially with the number of units in the system. That is, the system can stabilize any subset of active units in any column (feature or control column). The system inherits this property from the single column model (2) which can be shown to possess up to $(2^k - 1)$ stable stationary points (if k is the number of units in the column). The network state with maximal activity is the state in which all units in all columns are active. Stability in the network crucially depends on the level of inhibition within the individual columns, and this level is controlled by the parameter

ν in (3) and (4). If ν is increased, the number of stable stationary points decreases. The transitions of the stable states to unstable states occur around $\nu = 0.5$ which is the bifurcation point of the single column model (2) in the case of no input¹.

If ν in dynamics (3) and (4) gets larger, only activity configurations can survive in which active units sufficiently excite each other through their mutual connections. The dynamics thus selects the most stable subnets of active units from a large class of possible ones. The stability of these subnets is hereby determined by the internal connectivity of the network and by external feature input. In our system the internal connectivity allows for a comparison of activity distributions in feature columns (similarity term) and for an interaction between control columns that will be used to favor particular activation patterns (topology term). For low levels of inhibition, the system can potentially stabilize all activity configurations and we start with the state of maximal activity to allow for the selection of potentially any of them. Under the influence of noise, the state of maximal activity is, during an initial phase, automatically stabilized using zero inhibition ($\nu = 0$). Subsequently, we increase ν from a value $\nu_{\min} = 0.4$ that is smaller than the critical value of $\nu_c = 0.5$ to a value $\nu_{\max} = 0.6$ that is larger:

$$\nu(t) = \begin{cases} 0 & \text{if } \tilde{t} < T_{\text{init}} \\ (\nu_{\max} - \nu_{\min}) \frac{\tilde{t} - T_{\text{init}}}{T - T_{\text{init}}} + \nu_{\min} & \text{if } \tilde{t} \geq T_{\text{init}} \end{cases}, \quad (6)$$

where $\tilde{t} = t \bmod T$, which is $t - nT$, with n the greatest integer satisfying $t - nT \geq 0$. That is, after ν has reached its maximal value, the system is reset to full activity at $\nu = 0$ again, and the selection process can begin anew. Such a cyclically driven ν allows for repeated selections as required for changing inputs in realistic situations. One selection cycle, consisting of a reset to full activity and an increase of ν from ν_{\min} to ν_{\max} , will be called a ν -cycle (see Lücke and von der Malsburg, 2004).

4 Implementations of the Topology Constraint

To understand the effect of the topological term let us consider one-dimensional layers first. The connectivity among control columns is displayed in Fig. 4A for the case of layers with five instead of three nodes as in Fig. 2B. For simplicity we have chosen to just connect units that control strictly parallel links. Such a connectivity is reflected by the following form of the topology term in (5):

$$\mathcal{T}^{\mathcal{L}i, \mathcal{L}'j} = \sum_{a=-A}^A T_a \tilde{W}^{\mathcal{L}i+a, \mathcal{L}'j+a} \quad \text{with} \quad (T_a) = (\dots, u_2, u_1, 0, u_1, u_2, \dots), \quad (7)$$

where T_a is a one-dimensional kernel with u_i denoting positive connectivity strengths. $\tilde{W}^{\mathcal{L}i, \mathcal{L}'j}$ is the mean-free version of control column activity $W^{\mathcal{L}i, \mathcal{L}'j}$ given by $\tilde{W}^{\mathcal{L}i, \mathcal{L}'j} = W^{\mathcal{L}i, \mathcal{L}'j} - \frac{1}{N} \sum_l W^{\mathcal{L}i, \mathcal{L}'l}$. The sum over a is taken to continue cyclically

¹For $\nu = 0.5 - \epsilon$ the activities p_α possess stable states at $p_\alpha = 0.5 + \epsilon$ which results in a value of $h = 0.25 - \epsilon^2$ (compare Fig. 1).

if the index $(i + a)$ or $(j + a)$ exceeds the index range (compare Fig. 2B), i.e., the neighborhood relationship between control columns has the topological structure of a ring. Note that for Fig. 2B the maximal distance between connected columns, A , equals 1, and equals 2 in Fig. 4A. The connectivity given by (7) establishes mutual excitation between control units of parallel links. The situation is displayed in Fig. 5E for columns connected as in Fig. 4A. If a given control unit is active, it helps to keep active parallel links of its neighbors. Together with local inhibition within the control columns, this implements a competition between connectivity structures of parallel links. If the parameter ν is small enough, all these connectivity structures can co-exist. But if ν is increased, control units of structures which are only weakly supported by feature similarities are deactivated.

Fig. 4B illustrates connectivity that implements the topological constraint for two-dimensional layers. Only the connections for the central unit of the central column are shown. Note that for two-dimensions, the indices i and j in Eqns. (3) to (5) become two-dimensional ($i \rightarrow \vec{i}$ and $j \rightarrow \vec{j}$). The topology term in (5) now reads:

$$\mathcal{T}^{\mathcal{L}^{\vec{i}}, \mathcal{L}^{\vec{j}}} = \sum_{\vec{a}=(-A, -A)}^{(A, A)} T_{\vec{a}} \tilde{W}^{\mathcal{L}^{\vec{i}+\vec{a}}, \mathcal{L}^{\vec{j}+\vec{a}}} \quad (8)$$

with $(T_{\vec{a}}) = \begin{pmatrix} & & & \vdots & & & & & \\ & & & u_2 & & & & & \\ & & & u_1 & & & & & \\ \cdots & u_2 & u_1 & 0 & u_1 & u_2 & \cdots & & \\ & & & u_1 & & & & & \\ & & & u_2 & & & & & \\ & & & \vdots & & & & & \end{pmatrix},$

where $(T_{\vec{a}})$ is a two-dimensional kernel (empty entries are zero) in which the u_i denote positive connectivity strengths (compare Eqn. 12). For a given control unit $\tilde{W}^{\mathcal{L}^{\vec{i}}, \mathcal{L}^{\vec{j}}}$, the matrix $(T_{\vec{a}})$ contains the weights of all afferents from control units of neighboring parallel links. Fig. 4B illustrates the two-dimensional connectivity given by (8) for $A = 2$. In this case the potentially $(2A + 1)^2 = 25$ neighbors could be connected. However, for the kernel in (8) just the eight neighbors that correspond to the eight non-zero entries of $(T_{\vec{a}})$ are connected (black arrows in Fig. 4B)².

We have also tested a version of the system which includes diagonal connectivity between neighboring columns (corresponding to non-zero entries on the diagonals of $T_{\vec{a}}$), but have not observed significant functional advantages. We have therefore chosen to work with the kernel as described above as numerical simulations can be made more efficient in this case. Similarly to diagonal connections, a connectivity that involves connections between approximately parallel fibers has not produced significant functional improvements for the sets of natural images considered here (see below). In a system with one-dimensional layers as described in (Lücke and von der Malsburg, 2006), also approximately parallel links are interacting. There, feature vectors were artificial and independent from node to node. In the system

²Again we assume cyclic boundary conditions in the layers, such that the neighborhood relationship amongst the nodes in a layer now has the topological structure of a torus.

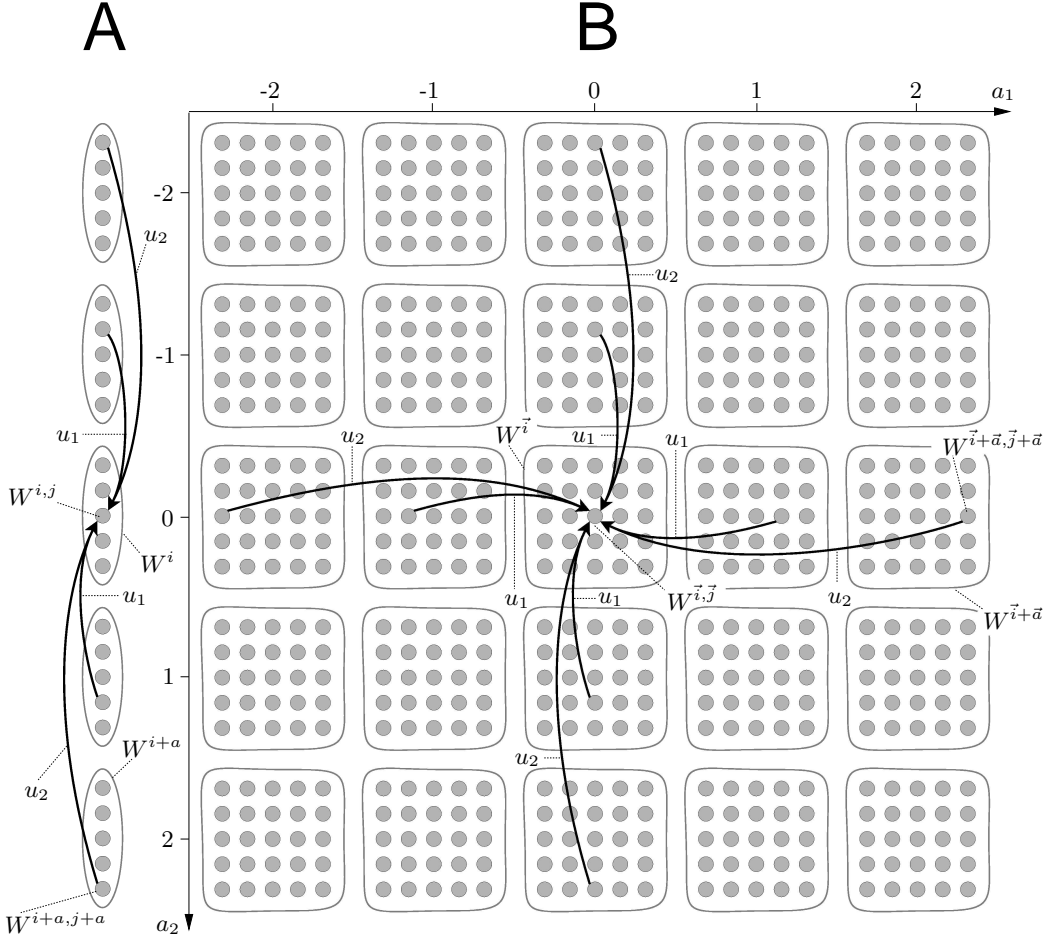


Figure 4: **A** Connectivity of control columns for one-dimensional input and model layers with five nodes each. All inputs received by the central unit of the central column are shown. Only units that control exactly parallel links are connected. Connectivity of any other unit is obtained by globally shifting the displayed connections while respecting cyclic boundary conditions (compare Fig. 2B). Note that in **A** and **B** the prefixes \mathcal{L} and \mathcal{L}' have been suppressed. W^i denotes the control column of node i and $W^{i,j}$ denotes its control unit with index j . The connectivity associated with the non-zero entries u_i of the kernel (T_a) in (7) is shown (black arrows). **B** Connectivity of control columns for two-dimensional input and model layers with 5×5 nodes each. In **B**, i and j become vectors \vec{i} and \vec{j} . All inputs received by the central control unit of the central column are shown. Again, the connectivities of any other unit can be obtained by globally shifting the displayed connections while respecting cyclic boundary conditions. Only units controlling exactly parallel links are connected. The connectivity associated with the non-zero entries u_i of the kernel $(T_{\vec{a}})$ in (8) is shown (black arrows).

described here we will use Gabor-wavelet filters as basis for our feature vectors. Consequently, neighboring feature vectors and the activity in their feature columns will not be independent. Control units of parallel links will be correlated also in the case in which only exactly parallel links are connected.

5 Feature Vectors

Let us neglect color and binocularity of the input and let the sub-populations of a column just be sensitive to different spatial frequencies and orientations, describing their receptive fields (RFs) by the well-known Gabor wavelets. Gabor wavelets describe the response properties of neurons in primary visual cortex (Jones and Palmer, 1987; Ringach, 2002) and are thought to be the basic constituents of natural images. They can be learned by a variety of algorithms, including ICA (Bell and Sejnowski, 1997) and sparse coding (Olshausen and Field, 1996). Note that Gabor-wavelets, indeed, also emerge if a system based on the dynamical column model as used in this paper is applied to natural images (Lücke, 2007). However, instead of learning them, we use a predefined set of Gabor wavelets for our purposes. To model the RFs of the sub-populations of our feature columns, we use Gabor filter responses as inputs. If V is an image with $V(\vec{x})$ denoting the gray-value of a pixel at position \vec{x} , the filter responses $Q_\alpha(\vec{x})$ are given by:

$$Q_\alpha(\vec{x}) = \int V(\vec{x}') \psi_\alpha(\vec{x} - \vec{x}') d^2 \vec{x}', \quad (9)$$

$$\psi_\alpha(\vec{x}) = \frac{k_\alpha^2}{\sigma^2} \exp\left(-\frac{k_\alpha^2 x^2}{2\sigma^2}\right) \left[\exp(i\vec{k}_\alpha \vec{x}) - \exp\left(-\frac{\sigma^2}{2}\right) \right], \quad \sigma = 2\pi, \quad (10)$$

where the wave vector is parameterized as

$$\vec{k}_\alpha = \begin{pmatrix} k_{\alpha x} \\ k_{\alpha y} \end{pmatrix} = \begin{pmatrix} k_\rho \cos \varphi_\mu \\ k_\rho \sin \varphi_\mu \end{pmatrix}, \quad k_\rho = 2^{(-\frac{\rho+2}{2})\pi}, \quad \varphi_\mu = \mu \frac{\pi}{8}, \quad (11)$$

with $\rho = 1, \dots, 5$ and $\mu = 1, \dots, 8$. That is, $(Q_1(\vec{x}), \dots, Q_{40}(\vec{x}))$ is a vector of Gabor-filter responses in which each entry corresponds to one of the 40 combinations of ρ and μ . As feature values we use the magnitude $\mathcal{J}_\alpha^{\mathcal{L}^i} = |Q_\alpha(\vec{x}_i)|$, thus ignoring Gabor phase to model complex cell responses (Hubel and Wiesel, 1977) (while appropriately sampling the spatial layer, with \vec{x}_i denoting the image position of node \mathcal{L}^i). As input to a feature column, (3), we use the mean-free version of $\mathcal{J}_\alpha^{\mathcal{L}^i}$ given by $\tilde{\mathcal{J}}_\alpha^{\mathcal{L}^i} = \mathcal{J}_\alpha^{\mathcal{L}^i} - \frac{1}{k} \sum_{\beta=1}^k \mathcal{J}_\beta^{\mathcal{L}^i}$ with $k = 40$. Feature vectors as defined by (9) to (11) have been used in various systems including Dynamic Link Matching (DLM) (Wiskott and von der Malsburg, 1995) and highly competitive applications to face and object recognition (e.g. Okada et al., 1998). For the formulation used here see (Wiskott et al., 1995). In applications using Gabor-features it has turned out that with 40, as above, good results can be achieved. Performance increases for more wavelets, but 40 represents a good compromise between performance and computational cost.

6 Simulations

To demonstrate the functioning of the system we use natural images of 512×512 pixels. Each input and each model image is covered by a grid of 8×8 nodes with cyclic boundary conditions (see Fig. 5A-D right images). Control columns are taken to be connected according to (8) with $A = 3$ and u_i given by:

$$u_i = \exp\left(-\frac{1}{2}\left(\frac{i}{A}\right)^2\right). \quad (12)$$

The exact values of the u_i 's are of subordinate importance for the simulation results but, in general, they should lie between 0 and 1 and should decrease with increasing i .

We numerically simulate the differential equations (3) and (4) with time steps of $\Delta t = \frac{1}{50}$ ms. The time constant a in (1) for the columnar dynamics (3) and (4) reflects the ability of the balanced network to rapidly stabilize new balanced states. In an earlier system with explicitly modeled spiking neurons (Lücke and von der Malsburg, 2004) the input sensitive transition from fully active columns to states with just one active unit was possible within a ν -cycle of $T = 25$ ms. For the abstract dynamics (3) and (4) with (1) this behavior is reproduced for time constants of roughly $a = 100 \text{ ms}^{-1}$ (compare Lücke and Bouecke, 2005) and same T (to reset the system we found that time intervals of about $T_{\text{init}} = 4$ ms are sufficient). We choose the noise term in (1) to be relatively small, $\sigma_n = 1 \times 10^{-7} \text{ ms}^{-1}$, and the input is taken to just weakly couple to the column dynamics $\kappa = 1.0 \text{ ms}^{-1}$ ($\kappa \ll a$) as in (Lücke and von der Malsburg, 2004), (Lücke, 2004) and (Lücke and Bouecke, 2005).

Input to a feature column potentially consists of feature vector input from its own layer and of input from feature columns of the other layer. After correspondences have been found, the direct connections between feature columns are crucial to convey image information between the layers in order to recognize or classify objects in later stages of processing (compare Olshausen et al., 1993). Fig. 3B illustrates how feature information can be transferred from one to the other layer. For the task of correspondence finding, as considered here, a direct exchange of information between feature columns is, however, not required. For simplicity, the feature layers thus solely communicate via their systems of control columns in the dynamics studied here. In a more general system, input to feature columns (see Eqn. 3) can, however, also constitute of mixtures of feature vector input and feature column input from the other layer (compare Lücke and von der Malsburg, 2006).

The system of control columns integrates feature information and information about the connectivity state between the layers. That is, control columns receive input from the evaluation of feature similarities between the layers and from neighboring control columns. Both input sources we take to be mixed using $C_I = 0.25$ in (5), i.e., the topology term is emphasized more than the similarity term.

For our simulations we visualize the activities of the control columns, i.e., the dynamic variables $W^{\mathcal{M}\vec{i},\mathcal{I}\vec{j}}$ and $W^{\mathcal{I}\vec{i},\mathcal{M}\vec{j}}$ in (4). The matrices $W^{\mathcal{M}\vec{i},\mathcal{I}\vec{j}}$ and $W^{\mathcal{I}\vec{i},\mathcal{M}\vec{j}}$ represent the connectivity from input layer \mathcal{I} to model layer \mathcal{M} and from \mathcal{M} to

\mathcal{I} , respectively. For *one-dimensional* layers the matrices W are two-dimensional and their visualization allows a direct interpretation of the inter-layer connectivity (compare Zhu and von der Malsburg, 2004; Lücke and von der Malsburg, 2006)³.

For *two-dimensional* input, $W^{\mathcal{M}^i, \mathcal{I}^j}$ and $W^{\mathcal{I}^i, \mathcal{M}^j}$ are four-dimensional matrices and, although their entries can in principle be visualized, the connectivities they represent are difficult to grasp intuitively. For two-dimensional images it is more instructive to visualize, for each control column, the center of gravity of its activity distribution. That is, we compute the position $\vec{y}_{\mathcal{L}^i}$ using:

$$\vec{y}_{\mathcal{L}^i} = \frac{\sum_{\vec{j}} W^{\mathcal{L}^i, \mathcal{L}'^j} \vec{x}_{\mathcal{L}'^j}}{\sum_{\vec{j}} W^{\mathcal{L}^i, \mathcal{L}'^j}}, \quad (13)$$

where the index \vec{j} runs over all 64 nodes of the 8×8 grid in \mathcal{L}' (see Fig. 5) and where $\vec{x}_{\mathcal{L}'^j}$ denotes these nodes' positions in the image. We will call $\vec{y}_{\mathcal{L}^i}$ the *mean link position* of control column $W^{\mathcal{L}^i}$. Note that the mean link position corresponds to a position in the image of the opposite layer \mathcal{L}' (compare Fig. 5E). We can therefore overlay this image with the mean link positions to better interpret the connectivity states. If finally just one control unit of node \mathcal{L}^i , say the unit with index \vec{j}_o , remains significantly active, Eqn. 13 results in $\vec{y}_{\mathcal{L}^i} \approx \vec{x}_{\mathcal{L}'^{\vec{j}_o}}$, i.e., the final mean position is close to the position of node $\mathcal{L}'^{\vec{j}_o}$ in this case. Fig. 5E illustrates this situation for one-dimensional images with one-dimensional 'grids' of five nodes each. Fig. 5A-D shows the time course of control column activities $W^{\mathcal{M}^i, \mathcal{I}^j}$ using the mean link positions of all control columns of the model layer for visualization. Grid points in the right column of images represent the node positions in the model image. For a given node's feature column $p^{\mathcal{M}^i}$, its grid position $\vec{x}_{\mathcal{M}^i}$ in the image is used to compute the Gabor-filter responses in (9). As mentioned earlier, the vector $\vec{J}^{\mathcal{M}^i}$ consists of the magnitudes of 40 such responses and encodes the image texture in an area around $\vec{x}_{\mathcal{M}^i}$. The mean link position (13) of each model node's control column is visualized in the left-hand-side images of Fig. 5A-D. Each model node in Fig. 5 has been assigned a different color (e.g., blue in the upper right and yellow in the lower left). The color identifies the node's grid position $\vec{x}_{\mathcal{M}^i}$ in the model image and its mean link position $\vec{y}_{\mathcal{M}^i}$ in the input image. When the system has converged to a final mapping, the active links connect points of the same color. In Fig. 5E the color coding is shown for one-dimensional images. For visualization purposes, we have connected any two mean link positions of directly neighboring control columns⁴. When all neighboring nodes have neighboring mean links, the visualization results in a more or less regular grid. Initially, in Fig. 5A, each model node is linked to all input nodes. Consequently, each mean link position is centered in the middle of the image. With increasing inhibition controlled by ν in (6), control units are deactivated and the activity in a control column is restricted to an increasingly small

³Final states of these systems are usually shifted diagonals which correspond to neighborhood-preserving connectivities.

⁴We did not visualize the cyclic neighborhood relationship (which would have resulted in all visualized positions having four edges) in order to make the translation of the grid in the input image with respect to the model grid more salient (compare Fig. 5E).

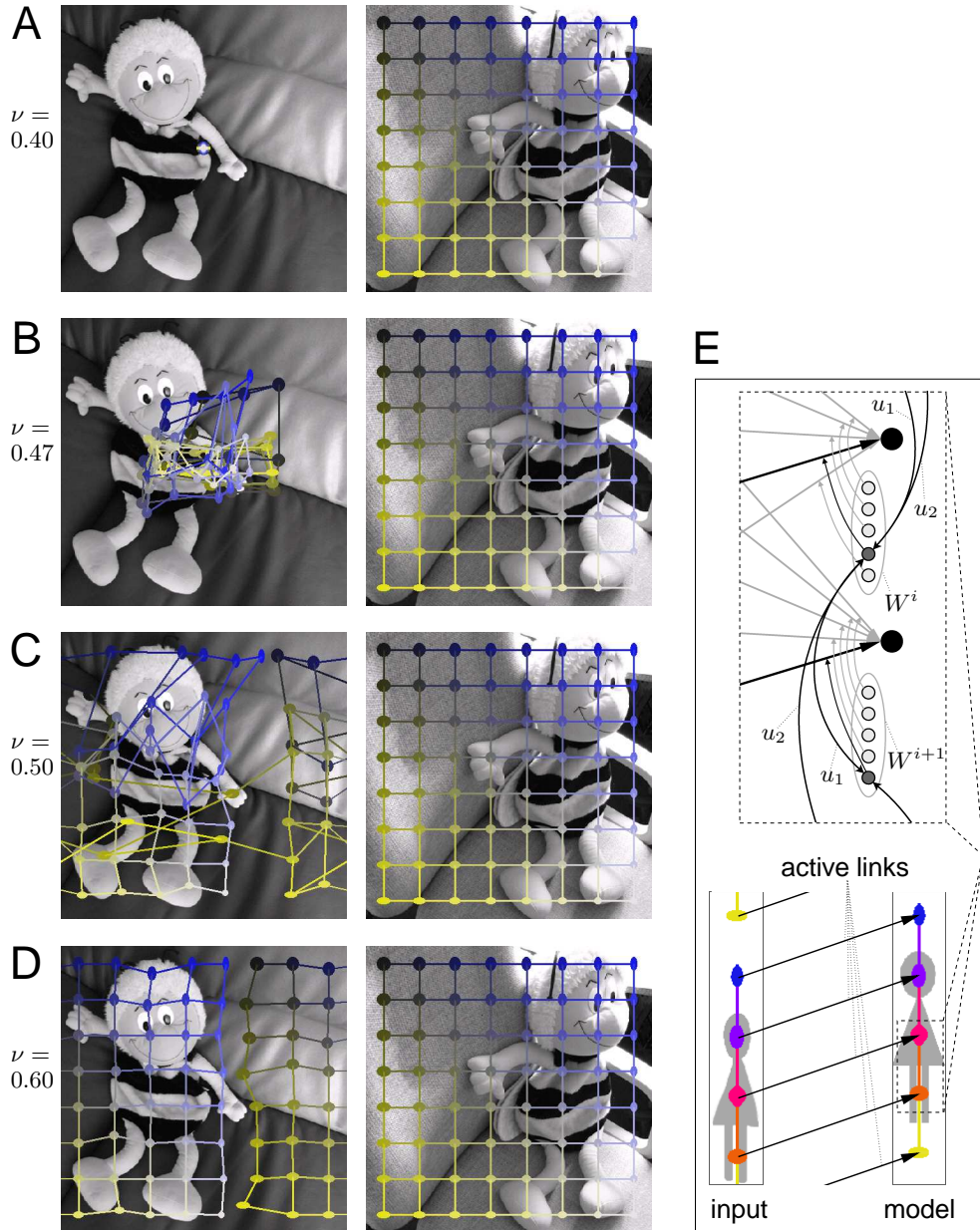


Figure 5: Time course of map formation between the feature layers. Grid points in the right image of **A-D** represent the node positions in the model layer. Each model node has active links originating from potentially many nodes in the input layer and the average of all active links, the mean link position (13), is shown on the left-hand-side of **A-D**. With increasing inhibition (increasing ν) links are deactivated and the map converges from all-to-all (**A**) to one-to-one connectivity that links corresponding points within the limit of grid resolution (**D**). To illustrate the color coding, **E** shows a mapping that has formed between one-dimensional ‘images’ (bottom). Two of the active links together with their control columns are shown in magnification (top). The displayed connections between the active control units (small dark circles) support the parallel links of the formed mapping (compare Fig. 4).

subset of units. In Fig. 5B this is reflected by the mean link positions starting to separate. In Fig. 5C the connectivity between the layers is already relatively sparse and, locally, neighboring control units in the model have often neighboring mean link positions in the input. In Fig. 5D the system has finally converged to a one-to-one connectivity structure in which the activities of the control columns are dominated by just one significantly active control unit each. The mean link positions, therefore, lie close to the grid-point positions of the input layer (compare Fig. 5E). The emergence of a regular grid puts in evidence that the final matrix $W^{\mathcal{M}\vec{i},\mathcal{I}\vec{j}}$ corresponds to a neighborhood-preserving connectivity from \mathcal{I} to \mathcal{M} . If ν is further increased, the mean link positions are approaching the fixed grid positions more closely. By inspecting Fig. 5D we may conclude that the system has found the right neighborhood preserving correspondence map within the limits of the grid resolution. Note that the system can, depending on the input, converged to any planar translation within this resolution. More precise results could be obtained with finer grids, although at higher computational costs. The time-course for the reciprocal mapping from model to input layer (given by $W^{\mathcal{I}\vec{i},\mathcal{M}\vec{j}}$) is very similar and results in the same correspondences.

During the formation of the correspondence map, the feature columns represent the Gabor feature-vectors by subsets of active feature units. With increasingly strong inhibition, these subsets of active units get smaller. First, the feature units with smallest inputs are deactivated and finally only subsets of units with strong input remain active. During map formation, there are, however, always many feature units active (compare Lücke and von der Malsburg, 2006). Only for very high levels of inhibition, and after the map has formed, just one unit per feature column remains active. In simulations, both, the representation of feature vectors by subsets of active feature units, and their deactivation times have been found to be important for map formation.

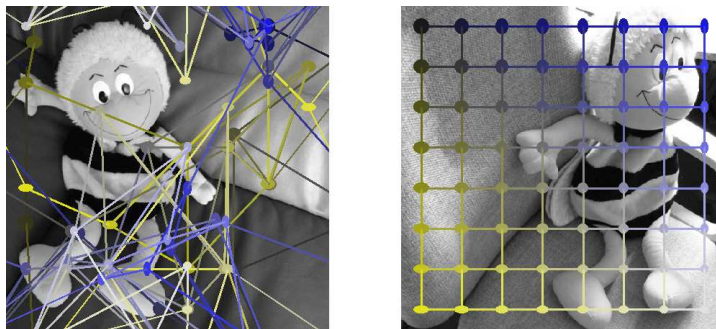


Figure 6: Result for the same image pair as used in Fig. 5 in the case of no topology term, i.e., C_I in (5) is equal one. The figure shows the connectivity for $\nu = 0.6$. Although the system was used with the same parameters otherwise, no correspondences were found.

The resulting mean link positions for the same simulation as in Fig. 5A-D but without the influence of the topological connectivity ($C_I = 1$) are shown in Fig. 6.

In this case, the system has not converged to a neighborhood-preserving connectivity as is obvious from the irregular grid on the left. Its emergence is caused by ambiguities in feature vector similarities if image and model differ too much, as is the case for the image pair in Fig. 6. This influence of ambiguities, and the importance of a topology constraint, are documented in (Wiskott, 1999). For the other extreme of only topological input ($C_I = 0$) the system converges, independent of the images, to a neighborhood-preserving connectivity that, however, does not connect corresponding points (see Lücke and von der Malsburg, 2006, for such simulations with 1D layers). Only if feature information and the topological constraint are appropriately mixed using intermediate values for C_I , the dynamics converges (in the limit of grid resolution) to the right correspondence map.

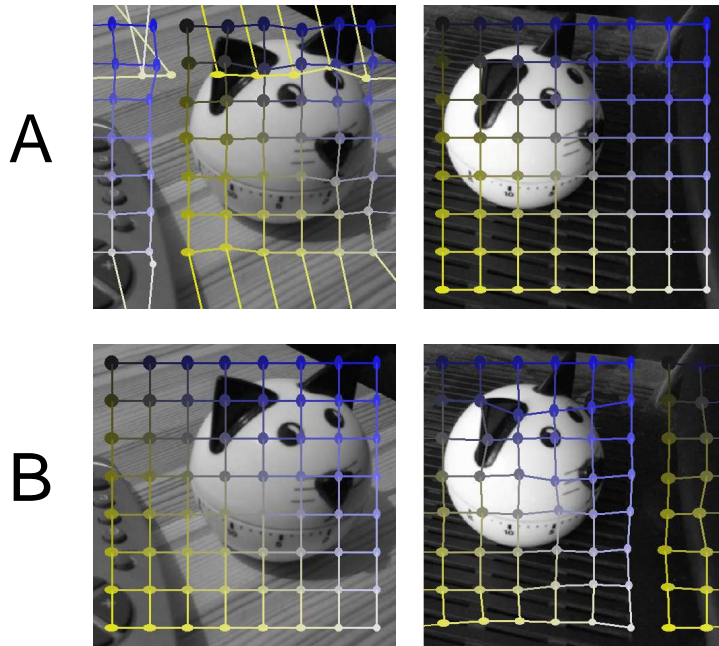


Figure 7: An example of convergence to an imperfect map between model and input layer. For the same system and parameters as in Fig. 5, we show connectivity matrices for $\nu = 0.6$ for both, input to model mapping ($W^{\mathcal{M}\vec{i}, \mathcal{I}\vec{j}}$) in **A**, and model to input mapping ($W^{\mathcal{I}\vec{i}, \mathcal{M}\vec{j}}$) in **B**. In **B** the dynamics has converged to a global neighborhood-preserving mapping but in **A** the mapping is imperfect as some wrong correspondences between background and object have developed.

The system has been simulated using various different image pairs. Accuracy of found correspondences can vary from image pair to image pair: highly distorted images of the same object and/or very different backgrounds can lead to the convergence to wrong correspondences. In general the network is, however, capable to find correspondences in pairs of very different images of the same object as illustrated by Fig. 5A-D or Fig. 7B.

To illustrate the convergence to a mapping that is not globally neighborhood

preserving consider Fig. 7A. The figure shows an imperfect match. Mean link positions of some control columns of the model layer show that the system has linked part of the background in the model to the object in the input. In this case, the lateral topological interaction has not been strong enough to force the system into a global neighborhood-preserving connectivity. However, correspondences of grid points on or in the vicinity of the object are found as accurately as permitted by grid resolution. Nodes at grid points on the background do actually not have correct correspondences if the backgrounds are different. In the case of Fig. 7A the feature dissimilarities between the background nodes have pushed some links out of the order of a regular mapping. If we use pairs of images that do not contain the same object, the emergence of irregular grids is the usual outcome.

7 Discussion

Finding homomorphic, that is, structure-preserving, mappings between neural feature layers — the correspondence problem — is a capability of fundamental importance for the brain, not only for the visual system (stereo matching, motion field extraction) or perceptual systems in general (invariant pattern recognition), but more fundamentally for the application of abstract schemas to concrete situations and analogical thinking, and thus for intelligence on all levels. By its very nature, correspondence requires for its establishment and expression neural implementation media for the formulation of structural relationships and for the expression of dynamic links. Both roles are played in our system by control columns.

Our model describes neural population activities by abstract continuous variables, but as shown in previous work (Lücke, 2005) this is capturing the essential properties of a more direct modeling of a system of spiking neurons (Lücke and von der Malsburg, 2004). The essential assumption of these systems is the existence of relatively disjunct populations of interconnected excitatory neurons. In combined neuroanatomical and neurophysiological measurements such populations were found in (Yoshimura et al., 2005). The relation of these populations to the mainly anatomically investigated cortical minicolumns (which motivated the modeling of self-excitatory populations in our earlier work) still has to be investigated, however (see, e.g., Peters and Yilmaz, 1993; Peters and Sethares, 1996; Buxhoeveden and Casanova, 2002, for experimental data on minicolumns).

Our model makes essential use of sigma-pi neurons, requiring sums of products of signals, *cf.* the first term in (5). Also the routing of information after correspondences are found has to rely on such mechanisms. Both cases involve control units, on the input side in one case, the output side in the other. The activity of control columns and of feature columns is described here by the same type of stochastic differential equations, Eqns. (3) and (4), but their connectivity patterns are markedly different. Control columns receive input from neighboring control units and, thus, form a network with lateral medium range connections. This network integrates input from afferents of inner- and extra-layer feature columns. The control column activity in this lateral network controls the inter-layer communication between fea-

ture columns. In our system this control is modeled to be local.⁵ These anatomical and neurophysiological characteristics may help to identify control units with known types of neurons⁶ whose functional roles have yet to be understood (Olshausen and Field, 2005). Feature columns, on the other hand, express local structure and must be able to transmit it over distance.

The facility for evaluating similarities of sets of neural signals in two feature columns makes it possible to represent whole feature spaces, instead of just single sample points as represented by sets of synaptic values in combination-coding neurons.

Note that in our model, neurons of both control and feature columns, receive only weak afferent input compared to input from within their own self-excitatory population (small coupling κ in Eqns. 3 and 4). Such weak couplings are consistent with physiological and anatomical studies (e.g. Douglas and Martin, 2004; Yoshimura et al., 2005), which report that cells in excitatory neural populations are much more strongly coupled to input from within their population than to medium and long-range afferent input. Our simulations show that such a system can, nevertheless, be very sensitive to external stimuli. Excitation and inhibition are kept in balance, but with increasing inhibition, afferent input can break the initial activity symmetry.

Our system solves several problems with previous models. One of them is the neural evaluation of feature similarities, which was a problem for (Zhu and von der Malsburg, 2004), (Olshausen et al., 1993) and (Wiskott and von der Malsburg, 1995). Another is excessive time requirement in (Wiskott and von der Malsburg, 1995). In the system presented, neural correspondence finding is possible in very small time intervals because of the use of a balanced network with population rates. The velocity of the system depends on the time required to deactivate neural populations. In simulations on the basis of single spiking neurons (Lücke and von der Malsburg, 2004), 25 ms have been found to be sufficient for these deactivations. The time constant a in Eqn. 1 has been chosen to reproduce those deactivation times in the abstract dynamics here used (compare Lücke, 2005; Lücke and Bouecke, 2005). The exact value of the time constant is difficult to determine as it can to some extent depend on details of neural time constants and connectivity within populations. However, even if neural spike and refraction times in (Lücke and von der Malsburg, 2004) are estimated conservatively, the length of the deactivation period is on the order of just a few tens of milliseconds. Thus, although difficult to determine exactly, the required order of magnitude for a that reproduces such deactivation times allows us to infer that convergence of the dynamics here presented is possible in times well below 100 ms.

In this paper we have considered pairs of images as input to our system. For each pair we have started from fully active control columns which corresponds to all-to-all connectivity between the feature layers. The cyclically changing inhibition (6) represents not only a mechanism that, by increasing inhibition, forces the system

⁵On the other hand, since a specific activated correspondence map constitutes valuable information in itself, as pointed out in (Arathorn, 2002), it might be advantageous for control neurons also to project over longer distances.

⁶For the hypothesis that control units are constituted by astrocytes see (Möller et al., 2007).

to converge but also a mechanism to reset the system after such a convergence. In a potential extension of the system, the cyclically driven inhibition could be exploited further: e.g., if the input is moving, it seems unrealistic to operate the system by resetting it to all-to-all connectivity multiple times in a second. Instead the map between the layers can partially be reset by preventing the inhibition (6) from dipping to low values during the oscillation. In this way the system would take the previously found correspondence as a prior for the next. Similarly, local distortions of objects could be addressed more actively: e.g., if a neighborhood preserving map between two images has been found after a first ν -cycle, the map could be refined by a partial reset and a second ν -cycle with less emphasis on the topology term in (5).

There are some more challenges ahead of us. Thus it is unrealistic to assume all links between the input layer and the model layer (which presumably are to be identified with primary visual cortex and infero-temporal cortex, resp.) to be direct. This would require a potentially unrealistic number of axons to converge on one unit. As proposed in (Olshausen et al., 1993), this problem is very likely solved in the brain with the help of intermediate layers to reduce the necessary fan-in and the number of required connections (Wolfrum and von der Malsburg, 2007). Further, whereas in the present system the model layer contains just one pattern that is to be compared to the image layer, the object recognition problem has to select the right model from a layer containing dozens of thousands of stored patterns. This will require a control hierarchy to load appropriate patterns into our model layer, and a bootstrap mechanism to overcome the simultaneous ambiguity of object *location* on the input side and object *identity* on the model side. Yet another important problem area is to develop a clear picture of the ontogenesis of the highly specific connectivity patterns required for our system.

Acknowledgments

We thank Yasser Roudi, Junmei Zhu, and Cornelius Weber for valuable comments on earlier versions of this manuscript and gratefully acknowledge funding by the Gatsby Charitable Foundation, the Hertie Foundation, and by the EU project FP6-2005-015803.

References

- Arathorn, D. (2002). *Map-Seeking circuits in Visual Cognition — A Computational Mechanism for Biological and Machine Vision*. Stanford Univ. Press, Stanford, California.
- Aristotle (1984). On memory. In Barnes, J., editor, *The Complete Works of Aristotle*, pages 714 – 720. Princeton Univ. Press, Princeton, New Jersey.

- Bell, A. J. and Sejnowski, T. J. (1997). The "independent components" of natural scenes are edge filters. *Vision Research*, 37(23):3327 – 38.
- Buxhoeveden, D. P. and Casanova, M. F. (2002). The minicolumn and evolution of the brain. *Brain, Behavior and Evolution*, 60:125–151.
- Dev, P. (1975). Perception of depth surfaces in random dot stereograms: a neural model. *International Journal of Man-Machine Studies*, 7:511–528.
- Douglas, R. J. and Martin, K. A. C. (2004). Neuronal circuits of the neocortex. *Annual Review of Neuroscience*, 27:419 – 451.
- Favorov, O. V. and Diamond, M. (1990). Demonstration of discrete place-defined columns, segregates, in cat SI. *Journal of Comparative Neurology*, 298:97 – 112.
- Hinton, G. E. (1981). A parallel computation that assigns canonical object-based frames of reference. In *Proc. IJCAI*, pages 683 – 685.
- Hubel, D. H. and Wiesel, T. N. (1977). Functional architecture of macaque visual cortex. *Proceedings of the Royal Society of London B*, 198:1 – 59.
- Jones, J. P. and Palmer, L. A. (1987). An evaluation of the two-dimensional Gabor filter model of simple receptive fields in cat striate cortex. *Journal of Neurophysiology*, 58(6):1233 – 1258.
- Kree, R. and Zippelius, A. (1988). Recognition of topological features of graphs and images in neural networks. *Journal of Physics A*, 21:813 – 818.
- Lücke, J. (2004). Hierarchical self-organization of minicolumnar receptive fields. *Neural Networks*, 17/8–9:1377 – 1389.
- Lücke, J. (2005). Dynamics of cortical columns – sensitive decision making. In *Proc. ICANN*, LNCS 3696, pages 25 – 30. Springer.
- Lücke, J. (2007). A Dynamical Model for Receptive Field Self-Organization in V1 Cortical Columns. *Proc. ICANN*, LNCS 4669, pages 389 – 398. Springer.
- Lücke, J. and Bouecke, J. D. (2005). Dynamics of cortical columns – self-organization of receptive fields. In *Proc. ICANN*, LNCS 3696, pages 31 – 37. Springer.
- Lücke, J. and von der Malsburg, C. (2004). Rapid processing and unsupervised learning in a model of the cortical macrocolumn. *Neural Computation*, 16:501 – 533.
- Lücke, J. and von der Malsburg, C. (2006). Rapid correspondence finding in networks of cortical columns. In *Proc. ICANN*, LNCS 4131, pages 668 – 677. Springer.

- Lücke, J., von der Malsburg, C., and Würtz, R. P. (2002). Macrocolumns as decision units. In *Proc. ICANN*, LNCS 2415, pages 57 – 62. Springer.
- Marr, D. and Poggio, T. (1976). Cooperative computation of stereo disparity. *Science*, 194:283–287.
- Messer, K., Kittler, J., Sadeghi, M., Hamouz, M., Kostin, et al. (2004). Face authentication test on the BANCA database. In *Proc. ICPR, Cambridge*, volume 4, pages 523 – 532.
- Möller, C., Lücke, J., Zhu, J., Faustmann, P. M., and von der Malsburg, C. (2007). Glial cells for information routing? *Cognitive Systems Research*, 8(1):28 – 35.
- Mountcastle, V. B. (1997). The columnar organization of the neocortex. *Brain*, 120:701 – 722.
- Okada, K., Steffens, J., Maurer, T., Hong, H., Elagin, E., Neven, H., and von der Malsburg, C. (1998). The Bochum/USC face recognition system and how it fared in the FERET phase III test. In Wechsler, H., Phillips, P., Bruce, V., F. Fogelman-Soulie, and Huang, T., editors, *Face Recognition : From Theory to Applications*, pages 186 – 205. Springer-Verlag.
- Olshausen, B. A., Anderson, C. H., and Essen, D. C. V. (1993). A neurobiological model of visual attention and invariant pattern recognition based on dynamic routing of information. *The Journal of Neuroscience*, 13(11):4700 – 4719.
- Olshausen, B. A. and Field, D. J. (1996). Emergence of simple-cell receptive field properties by learning a sparse code for natural images. *Nature*, 381:607 – 609.
- Olshausen, B. A. and Field, D. J. (2005). *23 Problems in Systems Neuroscience*, chapter What is the other 85% of V1 doing? Oxford University Press.
- Peters, A. and Sethares, C. (1996). Myelinated axons and the pyramidal cell modules in monkey primary visual cortex. *Journal of Comparative Neurology*, 365:232 – 255.
- Peters, A. and Yilmaz, E. (1993). Neuronal organization in area 17 of cat visual cortex. *Cerebral Cortex*, 3:49 – 68.
- Phillips, P. J., Moon, H., Rizvi, S. A., and Rauss, P. J. (2000). The FERET evaluation methodology for face-recognition algorithms. *IEEE Transactions on Pattern Analysis and Machine Intelligence*, 22(10):1090–1104.
- Ringach, D. L. (2002). Spatial structure and symmetry of simple-cell receptive fields in macaque primary visual cortex. *Journal of Neurophysiology*, 88:455 – 463.
- Thorpe, S., Fize, F., and Marlot, C. (1996). Speed of processing in the human visual system. *Nature*, 381:520 – 522.

- Wiskott, L. (1999). Role of topographical constraints in face recognition. *Pattern Recognition Letters*, 20(1):89–96.
- Wiskott, L., Fellous, J.-M., Krüger, N., and von der Malsburg, C. (1995). Face recognition and gender determination. International Workshop on Automatic Face- and Gesture-Recognition, Zürich, June 26-28, 1995.
- Wiskott, L. and von der Malsburg, C. (1995). Face recognition by dynamic link matching. In Sirosh, J., Miikkulainen, R., and Choe, Y., editors, *Lateral Interactions in the Cortex: Structure and Function*, chapter 4. www.cs.utexas.edu/users/nn/book/bwdraft.html. ISBN 0-9647060-0-8.
- Wolfrum, P. and von der Malsburg, C. (2007). What is the optimal architecture for visual information routing? *Neural Computation*, 19(12):3293 – 3309.
- Yoshimura, Y., Dantzker, J. L. M., and Callaway, E. M. (2005). Excitatory cortical neurons form fine-scale functional networks. *Nature*, 433:868 – 873.
- Zhu, J. and von der Malsburg, C. (2004). Maplets for correspondence-based object recognition. *Neural Networks*, 17/8–9:1311 – 1326.